Thin-Walled Structures 122 (2018) 83–89

Contents lists available at ScienceDirect

Thin-Walled Structures

journal homepage: www.elsevier.com/locate/tws

Full length article

Elastic buckling of externally pressurized Cassini oval shells with various shape indices

Jian Zhang[a,*], Weimin Wang[a], Fang Wang[b], Wenxian Tang[a], Weicheng Cui[b], Weibo Wang[c]

[a] School of Mechanical Engineering, Jiangsu University of Science and Technology, Zhenjiang 212003, China
[b] Shanghai Engineering Research Center of Hadal Science and Technology, Shanghai Ocean University, Shanghai 201306, China
[c] Chinese Ship Scientific Research Center, Wuxi, Jiangsu 214082, China

ARTICLE INFO

Keywords:
Cassini oval shell
Elastic buckling
Shape index
External pressure

ABSTRACT

This study examines the effect of shape index on the elastic buckling of Cassini oval shells under uniform external pressure. Shells are evaluated under a uniform wall thickness (2 mm) and capacity (3.63×10^6 mm^3), with the shape index, $k_c = c/a$, ranging from 0 to 0.99. Several numerical computations, involving linear elastic bifurcation analysis and geometrically nonlinear elastic analysis including eigenmode imperfections, are conducted for these shells. Some of them are investigated experimentally. The results show that a Cassini oval shell with a stable character seems to be an unfavorable shape due to its low load-carrying capacity, which is at variance with previous findings regarding this problem. Notably, the $k_c = 0.1$ Cassini oval geometry, exhibiting a high load-carrying capacity, appears to be a favorable shape in various fields such as underwater tanks, pressure hulls, and artificial capsules.

1. Introduction

Shells of revolution under uniform external pressure have long generated considerable research interest due to their effective load-carrying properties. They are applied in various engineering fields such as space launch vehicles [1], artificial capsules [2], buoyancy units [3], pressure hulls [4,5], and underground tanks [6]. The most extensively adopted configurations are spheres [7,8], cylinders [9,10], cones [11,12] and their combinations [13]. Atypical shells such as ellipsoids [14], barrels [15,16], eggs [17,18], and Cassini ovals [6] have been explored as well. However, these shells have been found to be prone to buckling when subjected to uniform external pressure, which often results in an unrecoverable collapse; the buckling of a vessel is heavily affected by its geometrical shape, wall thickness, and material properties, as well as the initial geometric imperfections [19–21].

One means of improving safety is to change the meridional shape of the shell. Numerous studies have focused on atypical shells of revolution with positive or negative Gaussian curvature. For instance, Blachut has performed a numerical and experimental study of the elastic–plastic buckling of a set of shells of revolution resembling circular arcs [22] and generalized ellipses [23], which were also compared with equivalent cylindrical shells. More recently, to resolve the disadvantages of spherical pressure hulls, such as high imperfection sensitivity, poor streamlining, and low space utilization rate, the buckling behaviors of egg-shaped shells were further studied [17], as well as the effect of shape index on buckling [18]. In addition, Jasion and Magnucki have carried out a numerical and analytical study of the elastic buckling of Cassini oval shells [6], clothoidal-spherical shells [24], and circular arc shells [25]. Notably, Jasion and Magnucki found that the equilibrium paths of some Cassini oval shells had a stable character [6], which is typical for elastic bars and plates. They suggested that the Cassini oval shells appeared to be a favorable shape for an externally pressurized structure, and that the Cassini oval shells could ensure safety both during buckling and in the postbuckling stages. However, only Cassini oval shells with shape indices within a limited range (0.6–0.9) were considered. Moreover, a comparison among shells that was based on the same capacity and mass led to a different wall thickness for each shell, which might reduce the convincingness of conclusions because most relevant comparisons were based on either the same capacity and wall thickness or the same mass and wall thickness [15,25].

Therefore, the current study focused on the elastic buckling of externally pressurized Cassini oval shells with shape indices within the range of 0–0.99. The shells were assumed to be of the same material, capacity, and wall thickness. The rest of this paper is organized as follows. Section 2 presents the definition of the geometry, load, capacity, wall thickness, material, and numerical model of Cassini oval shells. In Section 3, the linear elastic buckling behaviors of perfect Cassini oval shells and the nonlinear elastic buckling of imperfect shells

* Corresponding author.
E-mail address: zhjian127@163.com (J. Zhang).

http://dx.doi.org/10.1016/j.tws.2017.10.008
Received 7 May 2017; Received in revised form 25 July 2017; Accepted 3 October 2017
0263-8231/ © 2017 Published by Elsevier Ltd.

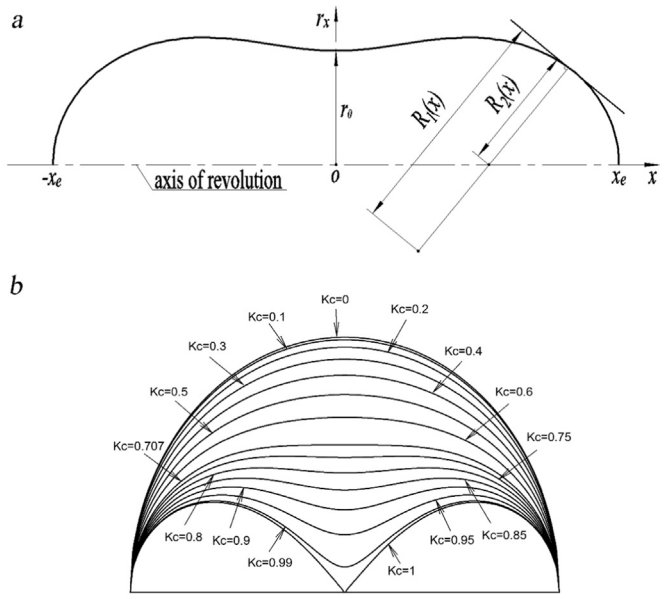

Fig. 1. Schematic of a Cassini ovaloidal shell (a), along with geometries with the typical shape indices, k_c (b).

are proposed on the basis of a number of numerical computations; the effect of shape index on buckling is also proposed. The computations revealed that Cassini oval shells with a stable character had a low load-carrying capacity. Notably, a Cassini oval shell with $k_c = 0.1$ exhibited a higher load-carrying capacity and lower imperfection sensitivity than a spherical shell in the case of elastic buckling and small eigenmode imperfection size-to-wall thickness ratio. This observation was partially validated for laboratory scale models and corresponding computations.

2. Problem definition

2.1. Geometrical properties

Consider a Cassini oval shell (Fig. 1(a)) with a semimajor axis, x_e, a semiminor axis, r_0, and a uniform wall thickness, t, subjected to some uniform external pressure, p_0; the radius, r_x, of the circumference of a shell of revolution in Cartesian coordinates is as follows:

$$r_x = \sqrt{\sqrt{4c^2x^2 + a^4} - (c^2 + x^2)}, \tag{1}$$

where a and c are equation parameters. The shape index, $k_c = c/a$, controls the shape of the Cassini oval shell. As shown in Fig. 1(b), for $k_c = 0$, a spherical shell is obtained. For $0 < k_c < 0.707$, a shell of revolution with positive Gaussian curvature is obtained. For $k_c = 0.707$, a clothoidal-spherical-like shell is obtained [24]. For $0.707 < k_c < 0.99$, a peanut-pod-like shell, including two individual small axisymmetric shells with positive Gaussian curvature along with the middle transition zone with negative Gaussian curvature, is obtained [26]. For $k_c = 1$, two individual water-drop-like shells with positive Gaussian curvature are obtained. According to this equation, the semimajor axis is $x_e = a\sqrt{1+k_c^2}$; the semiminor axis is $r_0 = a\sqrt{1-k_c^2}$.

The meridional radius $R_1(x)$ and circumferential radius $R_2(x)$ of the curvature of the Cassini oval shell can be obtained from Eq. (1), as follows:

$$R_1(x) = -\frac{[1+(dr_x/dx)^2]^{\frac{3}{2}}}{d^2r_x/dx^2}, \tag{2}$$

$$R_2(x) = r_x\sqrt{1+(dr_x/dx)^2}. \tag{3}$$

In addition, the capacity v of the Cassini oval shell is given by

Table 1
Geometrical parameters of Cassini oval shells, along with their linear, p_{LBA}, and nonlinear, p_{GNIA}, buckling loads.

k_c	a (mm)	c (mm)	r_0 (mm)	x_e (mm)	p_{LBA}(n) (MPa)	p_{GNIA} (k_{im}) (MPa)
0	95.343	0	95.343	95.343	1.420(12)	0.602(0.424)
0.100	95.503	9.550	95.024	95.979	1.382(11)	0.641(0.464)
0.200	95.999	19.200	94.059	97.900	1.287(11)	0.585(0.455)
0.300	96.878	29.063	92.416	101.144	1.110(10)	0.516(0.465)
0.400	98.229	39.292	90.028	105.796	0.900(10)	0.442(0.492)
0.500	100.198	50.099	86.773	112.024	0.678(9)	0.363(0.536)
0.600	103.021	61.812	82.417	120.142	0.452(7)	0.262(0.579)
0.707	107.455	75.971	75.994	131.598	0.243(5)	0.156(0.642)
0.750	109.836	82.377	72.649	137.294	0.170(5)	0.127(0.745)
0.800	113.216	90.573	67.929	144.987	0.107(4)	0.096(0.899)
0.850	117.482	99.860	61.888	154.189	0.083(3)	0.067(0.805)
0.900	123.019	110.717	53.623	165.506	0.060(2)	0.051(0.853)
0.910	124.330	113.141	51.548	168.104	0.110(2)	0.095(0.856)
0.920	125.725	115.667	49.274	170.838	0.195(2)	0.172(0.882)
0.930	127.211	118.306	46.758	173.721	0.312(4)	0.267(0.854)
0.940	128.799	121.071	43.943	176.769	0.320(4)	0.282(0.880)
0.950	130.500	123.975	40.749	180.000	0.344(4)	0.298(0.867)
0.960	132.327	127.034	37.052	183.434	0.377(3)	0.267(0.707)
0.970	134.296	130.267	32.648	187.096	0.368(3)	0.282(0.766)
0.980	136.426	133.697	27.148	191.015	0.419(3)	0.341(0.813)
0.990	138.738	137.350	19.571	195.226	0.618(3)	0.451(0.730)

Note: n = number of circumferential waves; $k_{im} = p_{GNIA}/p_{LBA}$.

$$v = 2\pi\int_0^{x_e} r_x^2 dx, \tag{4}$$

which, when combined with Eq. (1) and after integration [6] yields

$$v = \pi a^3\left[\frac{1}{2k_c}\ln\left(1 + 2k_c^2 + 2k_c\sqrt{1+k_c^2}\right) + \frac{1}{3}(1 - 2k_c^2)\sqrt{1+k_c^2}\right]. \tag{5}$$

In this study, Cassini oval shells with $0 < k_c < 0.99$ were evaluated with the same wall thickness $t = 2mm$ and capacity $v = 3.63\times10^6 mm^3$, directly determined using Eq. (5). The shape indices, equation parameters, and semimajor and semiminor axes were determined as listed in Table 1. To facilitate fabricating the laboratory scale models using rapid prototyping (RP) technique, it was assumed that shells were made of photosensitive resin. The material properties were assumed to be elastic, as follows: Young's modulus $E = 2510MPa$; Poisson's ratio $\mu = 0.41$.

2.2. Numerical computations

Serials of numerical computations were carried out for Cassini oval shells, involving linear elastic bifurcation analysis of perfect geometry and geometrically nonlinear elastic analysis with imperfections included of imperfect geometry. The former analysis was performed using the subspace iteration method whilst the later corresponded to the arc length method. All computations were conducted using the ABAQUS finite element system in line with ENV 1993-1-6 (2007) [27]. A fully integrated S4 shell element was employed to prevent hourglassing effect. Convergence studies of shells were carried out in the linear elastic bifurcation analysis [15,17,18,24], resulting in a total of 9600 elements for the numerical model.

The uniform pressure $p_0 = 1MPa$ was externally imposed on the whole surface of each Cassini oval shell. In this case, the eigenvalue obtained from the linear elastic bifurcation analysis corresponded directly to the linear buckling load, whereas the arc length value obtained from the nonlinear elastic analysis was equal to the nonlinear buckling load. Three spatial points of each model were constrained to avoid rigid body motion, which is identical to CCS2013 [28] as follows: Uy = Uz = 0, Ux = Uy = 0, Uy = Uz = 0. These boundary conditions led to no excessive constraint due to the uniformly imposed pressure.

In addition, for the nonlinear elastic analysis, the eigenmode

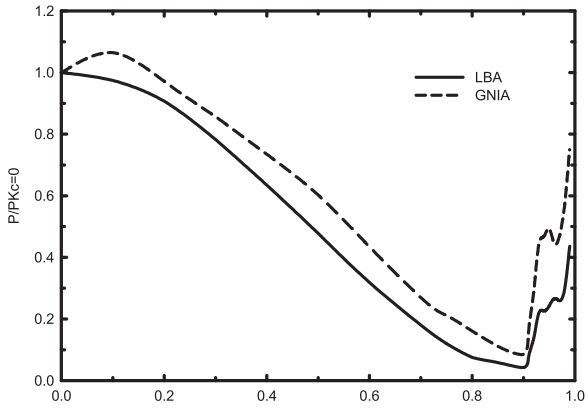

Fig. 2. Plot of the linear buckling load, p_{LBA}, and the nonlinear buckling load, p_{GNIA}, versus the shape index, k_c.

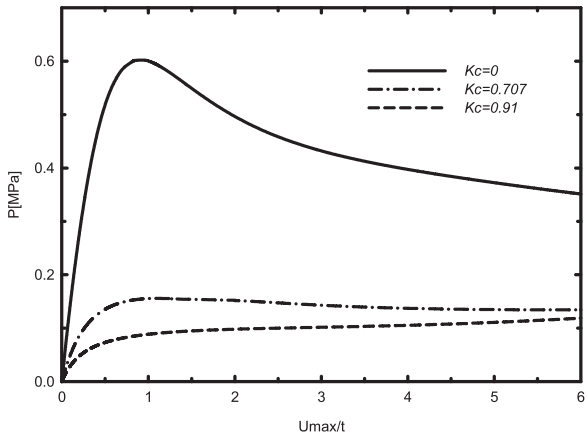

Fig. 3. Equilibrium paths of Cassini ovaloidal shells with the typical shape indices, k_c.

imperfection obtained from the corresponding linear elastic bifurcation analysis was introduced into the perfect model, which had been extensively adopted to conservatively evaluate the load-carrying capacity of shells of revolution in the preliminary design stage [27,29]. The imperfection size-to-wall thickness ratio was assumed to be 0.4. Table 1 and Figs. 2 and 3 detail the results obtained from the numerical computations.

3. Results and discussion

3.1. Linear elastic bifurcation analysis

The linear elastic buckling behaviors of Cassini oval shells are fundamentally affected by the shape index, k_c. As presented in Table 1 and Fig. 2, the linear buckling load, p_{LBA}, first decreased monotonically with an increase in the shape index due to the decreasing meridional curvature. This observation is similar to those of previous studies conducted on the buckling of Cassini oval shells in the range $0.6 \leq k_c \leq 0.9$ [6]. Notably, after an inflection point ($k_c = 0.9$), a significant increase in the buckling load was observed, probably because the buckling behaviors of Cassini oval shells in this range are mainly determined by two individual small axisymmetric shells. The meridional curvature of these small shells rapidly increased with the shape index. Nevertheless, some fluctuations in the buckling load were observed, possibly because of the negative Gaussian curvature of the middle transition zone connecting the two small shells. Comparable fluctuations were also found in a previous study [6].

The linear buckling modes of the Cassini oval shells within the range $0 \leq k_c < 0.9$ were identical and took the shape of a number of circumferential waves (n), along with one longitudinal half-wave (m = 1), which is typical for shells of revolution with positive Gaussian curvature [15,24]. The linear buckling modes in the range $0.9 \leq k_c \leq 0.92$, were in the form of two circumferential waves and one longitudinal half-wave. After this range, the linear buckling modes of the Cassini oval shells degenerated into the linear buckling modes of two individual small axisymmetric shells, each with positive Gaussian curvature. The higher the linear buckling load was, the more the number of circumferential waves was. The higher the meridional curvature was, the more the number of circumferential waves is.

3.2. Geometrically nonlinear elastic analysis with imperfections included

As with the linear elastic bifurcation analysis, the shape index, k_c, of imperfect Cassini oval shells fundamentally affects their nonlinear elastic buckling behaviors. As shown in Table 1 and Fig. 2, the relationship between the critical buckling load, p_{GNIA}, and the shape index was nearly the same as the corresponding relationship of the perfect Cassini oval shells, except for the $k_c = 0.1$ case. This exception is detailed later in this section. For $0 \leq k_c \leq 0.8$, the ratio of the critical buckling load, p_{GNIA}, to the linear buckling load, p_{LBA}, significantly increased with the shape index. This suggests that the higher the shape index is, the less sensitive to shape deviation the critical buckling load is. However, for $k_c > 0.8$, no obvious relation was determined between the critical buckling load and the shape index, as the buckling behaviors of Cassini oval shells in this range are strongly influenced by the geometry of their middle zones along with the complicated eigenmode imperfections.

The equilibrium paths of imperfect Cassini oval shells, plotted as the applied load, p, versus the maximum deflection-to-wall thickness ratio, u_{max}/t, indicated whether the structure is stable or not after the critical point. The deflection, u_{max} was measured on the maximum deflection point of shell, which was found at the end of the path. This choice was due to the fact that the selected point located at the collapse zone of the shell considered. According to the relationship between the applied load and the deflection of this point, one can evaluate the character of the shell after buckling. The obtained paths can be divided into three types as follows: the unstable (type 1), metastable (type 2), and stable (type 3) paths. Typical examples of these paths can be seen in Fig. 3. First, unstable paths (type 1) were found for shells in the range $0 \leq k_c < 0.707$, where the applied load first increased monotonically with an increase in the deflection up to the peak value (the critical buckling load), beyond which the applied load decreased; for example, the $k_c = 0$ imperfect Cassini oval shell in Fig. 3 demonstrates this pattern. This is the typical character for shells of revolution with positive Gaussian curvature under external uniform pressure [30]. Furthermore, the slope of the postbuckling line increased with a decrease in the shape index. Second, metastable paths (type 2) were found for shells at $k_c = 0.707$ and in the range $0.94 \leq k_c \leq 0.99$, where the applied load first increased monotonically with an increase in the deflection up to the peak value (the critical buckling load), and then nearly leveled off; an example of this is the $k_c = 0.707$ imperfect Cassini oval shell depicted in Fig. 3.

Finally, stable paths (type 3) were found for shells in the range $0.75 \leq k_c \leq 0.93$, where the applied load first increased monotonically with an increase in the deflection up to the inflection point (the critical buckling load), beyond which a relative increase was observed in the applied load; an example of this is the $k_c = 0.91$ imperfect Cassini oval shell shown in Fig. 3. These findings confirmed the previous results [6] and seem to be encouraging. However, it must be noted that despite these shells exhibiting a stable character, their critical buckling loads, reflecting load-carrying capacities, are very small compared with those of barreled shells ($0 \leq k_c < 0.4$), particularly for spherical shells ($k_c = 0$) and nearly spherical shells ($k_c = 0.1$). For engineering applications, Cassini oval shells in this range appear to be an unfavorable shape for a shell structure under external pressure, because a relatively high carrying load may lead to excessive shell deformation. In addition, the critical buckling modes of imperfect Cassini oval shells at the peaks or

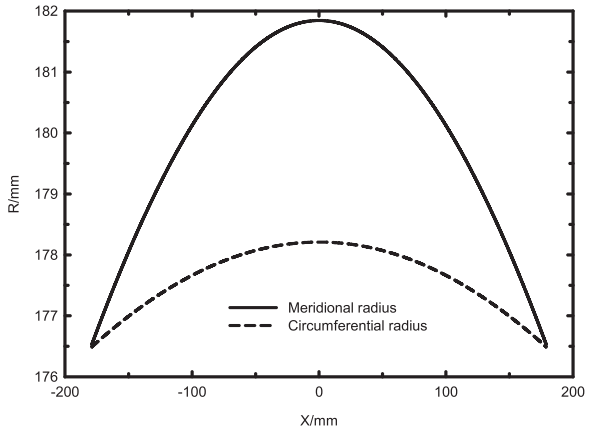

Fig. 4. Meridional and circumferential radii of the $k_c = 0.1$ imperfect Cassini oval shell.

inflection points of the paths were similar to the linear buckling modes of perfect shells, because of the introduction of eigenmode imperfections. The postbuckling modes also had one or more indentations, which is typical for imperfect shells of revolution under external uniform pressure [31–33].

Notably, according to Table 1 and Fig. 2, the critical buckling load of the nearly spherical shell ($k_c = 0.1$) was approximately 5.5% higher than that of the spherical shell ($k_c = 0$), although its linear buckling load was slightly less than that of the spherical shell. This may be due to the fact that the nearly spherical shell with a slightly asymmetric geometry was less sensitive to shape imperfection than the spherical shell with a highly symmetric geometry. Moreover, as illustrated in Fig. 4, the meridional radius in the middle zone (equator) of the nearly spherical shell ($k_c = 0.1$) was slightly greater than the radius of the spherical shell (180 mm), whereas the meridional radius in the remaining zone, as well as the circumferential radius in the whole range, was less than 180 mm. To confirm this notable phenomenon, four small imperfection size-to-wall thickness ratios, namely 0.1, 0.2, 0.3, and 0.4, were examined for the buckling of nearly spherical and spherical shells. A similar phenomenon can be identified in Fig. 5, confirming that the load-carrying capacity of the $k_c = 0.1$ imperfect Cassini oval shell could be higher than that of the equivalent spherical shell with a smaller imperfection size-to-wall thickness ratio. In addition, the spherical shell for each imperfection size-to-wall thickness ratio collapsed in the form of an elliptical local dent. The ratio of the major axis, a, to the minor axis, b, increased with an increase in the imperfection size-to-wall thickness ratio (parenthetical quantity in column 6 of Table 2), indicating that a nearly perfect spherical shell with a small imperfection size-to-wall thickness ratio collapses in the form of a nearly circular

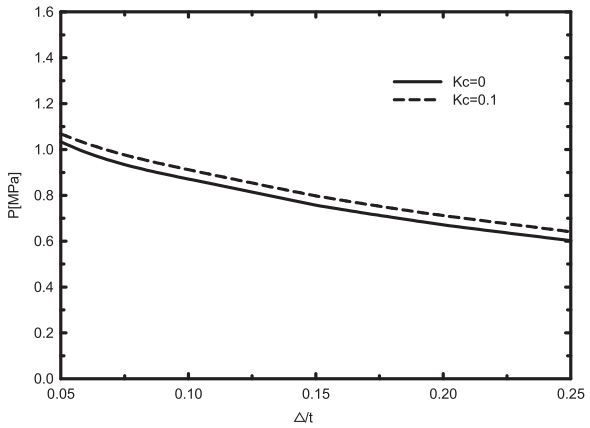

Fig. 5. Critical buckling loads of the $k_c = 0$ and $k_c = 0.1$ imperfect Cassini oval shells versus the imperfection size-to-wall thickness ratio, Δ/t.

local dent. The parenthetical quantity in the last column of Table 2 reveals that the predicted equivalent radius of a local dent, $\bar{r} = \sqrt{ab}$, is in good agreement with the radius r obtained from the empirical equation [32]:

$$r = \sqrt{R_0 H - H^2/4}, \tag{6}$$

where R_0 is the radius of the spherical shell, and H is the depth of the local dent obtained from numerical results, a is the major axis of the dent whist b is the minor axis.

It is inferred that a $k_c = 0.1$ Cassini oval shell can be applied in various engineering situations such as underwater tanks and pressure hulls of shallow submersibles or submarines, along with artificial capsules subjected to external pressure. In these situations, thin-walled shells that inevitably have small shape imperfections are often designed to withstand as much load as possible; buckling may be the main influencing factor in such designs. In addition, it may be boldly assumed that many spheroidal natural organisms, such as biological cells [34,35], pollen grains [36,37], and virus capsules [2,38], may have a nearly spherical configuration – they may be Cassini oval shells with very small shape indices, which can support considerably high loads and collapse in the elastic range. The assumption requires further validation.

3.3. Experimentation

To experimentally check the effectiveness of the $k_c = 0.1$ Cassini oval shell, six laboratory scale models were tentatively fabricated, measured and tested in this section. Three of them were nominally identical $k_c = 0.1$ Cassini oval shells, the others were nominally identical $k_c = 0$ Cassini oval shells (spherical shells). Their nominal sizes are listed in the first three rows of Table 1.

Shells were fabricated upright along the axis of revolution via Stereo Lithography Appearance (SLA), which was based on the corresponding three-dimensional CAD models with perfect geometry. All of them were manufactured during the same building, then cleaned and post cured at the same time. A fine point support was employed to ensure greater surface finish. In order to easily get rid of the support inside shells after the fabrication, two small circular holes ($2\alpha = 8^\circ$) with the radius of 6.75 mm were designed at two poles for each model, an example of the $k_c = 0$ Cassini oval shell is shown in Fig. 6(a). Photosensitive resin was applied to fabricate shells, which had a Young's modulus of $E = 2510$MPa, a Poisson's ratio of $\mu = 0.41$, a yield strength of 33 MPa and a mass density of 1130 kg/m^3.

Prior to test, the outer surface of each fabricated shell was precisely measured through a three-dimensional optical scanner (Open Technologies Corporation, $\leq$ 0.02 mm). In this way, the CAD models for shells can be obtained, which included deterministic geometric imperfections imparted through the fabrication. Radius deviations of each shell, indicating the geometric imperfections, are show in Fig. 7. As can be seen, very small difference between the fabricated and perfect shells was obtained, suggesting good repeatability and precision of the fabrication.

After the measurements, each hole was tightly covered and strengthened using a small carbon fiber reinforced composite cap. This kind of composite material was much stronger than photosensitive resin. The cap had a wall thickness of about 2 mm, and an arc angle of $2\beta = 37^\circ$, an example of the $k_c = 0$ Cassini oval shell is shown in Fig. 6(b). In this case, water could not fill into shells, and the effect of holes on the shell buckling was minimized during the test. Then, shells were slowly pressurized to collapse in a pressure vessel. The vessel had an inner diameter of 200 mm, a total length of 1000 mm, a maximum pressure of 20 MPa, and used water as the pressurizing medium. The pressure inside the vessel was recorded using a pressure transducer, and controlled by a hand-operated pump. All shells tended to collapse suddenly with a significant decrease in pressure. After the tests, each

Table 2
Geometrical parameters of local dents of the imperfect spherical shells.

Δ(mm)	H (mm)	R_0 (mm)	r (mm)	a (mm)	b ($\sqrt{ab}$) (mm)	$\bar{r}$ ($\bar{r}/r$) (mm)
0.1	10.75	95.34	31.56	63.08	61.49(1.03)	31.14(0.987)
0.2	11.15	95.34	32.12	65.55	63.33(1.04)	32.22(1.003)
0.3	12.08	95.34	33.39	69.01	63.36(1.09)	33.06(0.990)
0.4	12.75	95.34	34.28	72.44	64.59(1.12)	34.20(0.998)
0.5	13.10	95.34	34.73	75.85	63.37(1.20)	34.66(0.998)

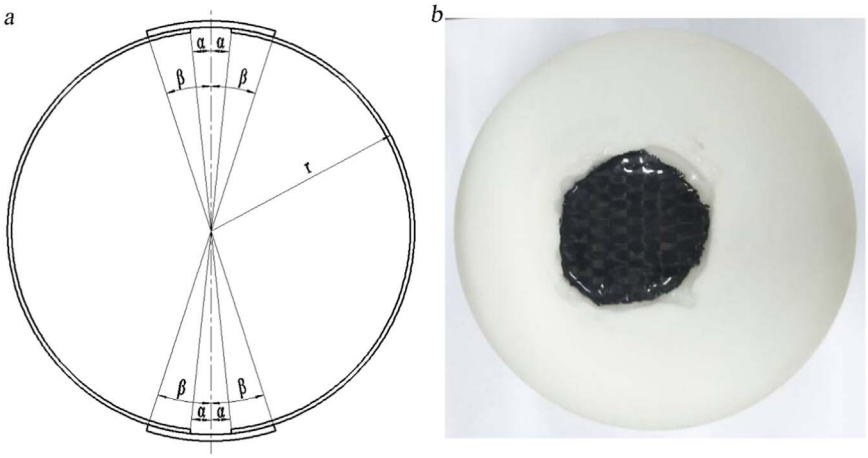

Fig. 6. Schematic representation of an experimental $k_c = 0$ Cassini oval shell (a) and the corresponding fabricated photograph (b).

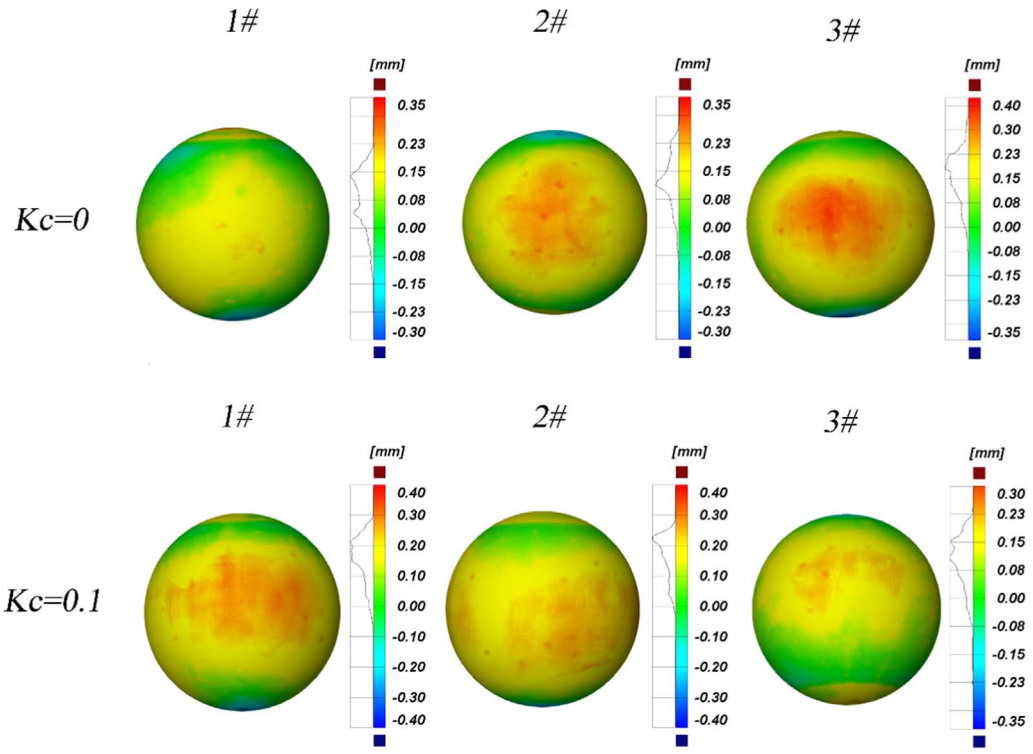

Fig. 7. Radius deviations of fabricated $k_c = 0$ Cassini oval shells from the perfect geometry, along with $k_c = 0.1$ Cassini oval shells.

collapsed shell was fetched out from pressure vessel. The wall thickness of each shell was measured using a micrometer gauge. The testing and measuring results are given in Table 3 and Fig. 8, showing the reasonable repeatability of experiments.

As listed in the table, the collapse pressure of $k_c = 0$ Cassini oval shells varied from 0.899 to 0.949, which might result from variations in wall thickness and shape deviation (Fig. 7). The similar trend could be found for $k_c = 0.1$ Cassini oval shells. However, the average collapse pressure (0.925 MPa) of $k_c = 0$ Cassini oval shells was 7.6% lower than that (0.996 MPa) of $k_c = 0.1$ Cassini oval shells. This finding confirmed that in the case of small geometric imperfections the $k_c = 0.1$ Cassini oval shell had a better load carrying capacity than the equivalent spherical shell. In addition, as observed in Fig. 8, shells collapsed in the form of local fracture due to the brittleness of parent material. The collapse location was relatively random, which might be attributed to the random variations in fabricating thickness and shape deviation.

Table 3
Measured thicknesses, tested collapse loads of $k_c = 0$ and $k_c = 0.1$ Cassini oval shells, along with corresponding numerical loads.

Sample	$k_c = 0$			$k_c = 0.1$		
	1#	2#	3#	1#	2#	3#
$t_{max}\,[mm]$	1.992	2.000	1.978	2.011	2.011	1.991
$t_{min}\,[mm]$	1.934	1.690	1.895	1.901	1.943	1.889
$t_{ave}\,[mm]$	1.940	1.930	1.970	1.965	1.979	1.940
$P_{test}\,[MPa]$	0.899	0.949	0.927	0.973	1.066	0.948
$P_{numerics}\,[MPa]$	0.895	0.907	0.871	0.957	0.990	0.934
$P_{numerics}/P_{test}$	0.996	0.956	0.940	0.984	0.929	0.986

3.4. Numerical analysis of tested shells

To further study the buckling of tested shells and benchmark the nonlinear numerical computations implemented in Section 2.2, the geometrically nonlinear elastic analysis was performed for above six fabricated $k_c = 0.1$ and $k_c = 0$ Cassini oval shells. This was done using the arc length method available in ABAQUS code.

Mesh was generated uniformly and freely on each measured geometry, including initial deterministic geometrical imperfections caused by the fabrication. Shell element S4 was mainly chosen to avoid hourglassing together with a few S3 shell elements. Mesh convergence studies resulted in 16490 S4 elements and 502 S3 elements for the 1# $k_c = 0$ shell, 16449 S4 elements and 574 S3 elements for the 2# $k_c = 0$ shell, 16422 S4 elements and 780 S3 elements for the 3# $k_c = 0$ shell, 16191 S4 elements and 412 S3 elements for the 1# $k_c = 0.1$ shell, 16021 S4 elements and 578 S3 elements for the 2# $k_c = 0.1$ shell, 16340 S4 elements and 580 S3 elements for the 3# $k_c = 0.1$ shell.

The elastic material modelling was assumed with the same properties as Section 2.2. The wall thicknesses were assumed to the average measured results in Table 3. For the each numerical model, two reinforced composite caps covered on the corresponding holes were also introduced with nominal geometry to simulate the strengthening effect. The properties of the composite material were set as follows: Young's modulus $E = 10000$MPa; Poisson's ratio $\mu = 0.302$. In addition, the load and boundary conditions were similar to Section 2.2. The obtained results were given in Table 3 and Fig. 8.

As can be seen from the table, the numerical buckling load, $p_{numerics}$, varied from 0.871 to 0.907 for the $k_c = 0$ Cassini oval shells, and from 0.934 to 0.990 for the $k_c = 0.1$ Cassini oval shells. The predicted value is 92.9–99.6% of the tested one, suggesting a reasonable agreement and a relatively precise computation. This small difference between theory and experiment could be associated with the average wall thickness assumption. These findings confirmed the previous experimental results in Section 3.3 that the Cassini oval shell had a better load carrying capacity than the equivalent spherical one. Furthermore, the equilibrium paths of all shells behaved an unstable character, which was similar to the $k_c = 0$ Cassini oval shell in Fig. 3. The post buckling modes at the end of the paths took the form of a local dent, which agreed well with the experimental ones.

4. Conclusions

This paper presents the results of a numerical and partially experimental study of the elastic buckling of Cassini oval shells subjected to uniform external pressure, along with the effect of the shape index on such buckling. A detailed comparison between $k_c = 0.1$ Cassini oval and spherical shells is made as well.

The study results reveal that the linear buckling load of a geometrically perfect Cassini oval shell first decreased monotonically with an increase in the shape index, but after an inflection point ($k_c = 0.9$), the buckling load increased substantially, although some fluctuations

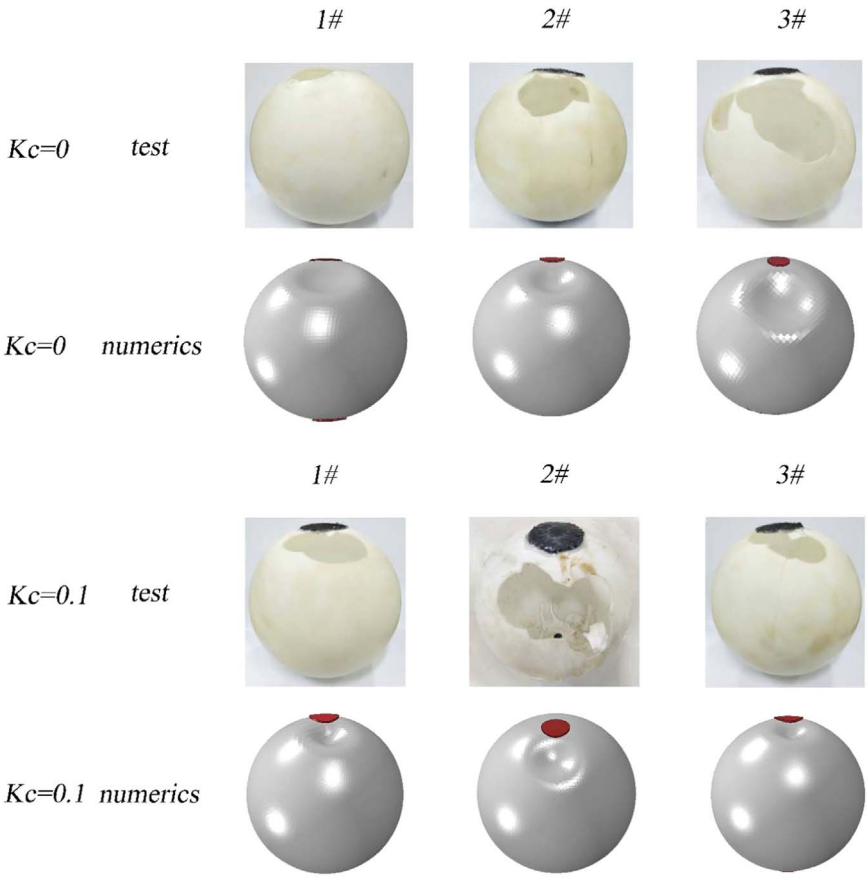

Fig. 8. Collapse modes of $k_c = 0$ and $k_c = 0.1$ Cassini oval shells after test, along with numerical results.

existed. The linear buckling modes took the form of a number of circumferential waves and one longitudinal half-wave in the whole or local surface. These findings are similar to those of previous studies [6,15,24].

The relation between the critical buckling load of a geometrically imperfect Cassini oval shell and its shape index was nearly the same as the relation of the perfect Cassini oval shell and its shape index, except for the $k_c = 0.1$ Cassini oval shell. For $0 \leq k_c \leq 0.8$, the higher the shape index was, the less sensitive to shape deviation the critical buckling load was. By contrast, for $k_c > 0.8$, no obvious relation was observed. The equilibrium paths of imperfect shells can be divided into three types, namely the unstable, metastable, and stable paths. Although some shells exhibited a stable character, their load-carrying capacities were very low.

Notably, the critical buckling load of the nearly spherical shell ($k_c = 0.1$) was even higher than that of the spherical one ($k_c = 0$) due to the effects of imperfection sensitivity, circumferential radius, and meridional radius. This finding was obtained from various small imperfection size-to-wall thickness ratios, validated against experimental results and the corresponding computations. This indicates that the $k_c = 0.1$ Cassini oval geometry, which exhibited a high load-carrying capacity, has potential applications in various fields such as underwater tanks, pressure hulls, and artificial capsules.

However, some limitations of this study are worth noting. Although our findings are encouraging, only eigenmode geometric imperfection was taken into account. Future work should examine other types of imperfections such as local dimples or axisymmetric dimples. Additionally, the wall thickness of each shell in this work was assumed to be constant. It may be beneficial to investigate cases in which the wall thickness varies in the meridional direction.

Acknowledgments

The authors acknowledge the support provided by the Natural Science Foundation of Jiangsu Province under the title of "Bionic Study into Deep Pressure Hulls Based on Biological Properties of Eggshells" (Grant No. BK20150469), by the Key Program of the National Natural Science Foundation of China under the title of "Structural Reliability Analysis on the Spherical Hulls of Deep-sea Manned Submersibles" (Grant No. 51439004), and by the General Program of the National Natural Science Foundation of China under the title of “Study on the Design and Life Calculation Method for the Managing Steel Spheres of Full-ocean-depth Manned Submersibles” (Grant No. 51679133).

References

[1] J. Błachut, Buckling of composite domes with localised imperfections and subjected to external pressure, Compos. Struct. 153 (2016) 746–754, http://dx.doi.org/10.1016/j.compstruct.2016.07.007.
[2] S. Knoche, J. Kierfeld, Buckling of spherical capsules, Phys. Rev. E - Stat. Nonlinear, Soft Matter Phys. 84 (2011), http://dx.doi.org/10.1103/PhysRevE.84.046608.
[3] J. Blachut, K. Magnucki, Strength, stability, and optimization of pressure vessels: review of selected problems, Appl. Mech. Rev. 61 (2008) 060801, http://dx.doi.org/10.1115/1.2978080.
[4] S.S. Datta, S.H. Kim, J. Paulose, A. Abbaspourrad, D.R. Nelson, D.A. Weitz, Delayed buckling and guided folding of inhomogeneous capsules, Phys. Rev. Lett. 109 (2012), http://dx.doi.org/10.1103/PhysRevLett.109.134302.
[5] B.B. Pan, W.C. Cui, An overview of buckling and ultimate strength of spherical pressure hull under external pressure, Mar. Struct. 23 (2010) 227–240.
[6] P. Jasion, K. Magnucki, Elastic buckling of Cassini ovaloidal shells under external pressure – theoretical study, Thin-Walled Struct. 67 (2015) 179–192.
[7] B.B. Pan, W.C. Cui, A comparison of different rules for the spherical pressure hull of deep manned submersibles, J. Ship Mech. 15 (3) (2011) 276–285, http://dx.doi.org/10.1016/j.marstruc.2010.07.005.
[8] J. Zhang, M. Zhang, W. Tang, W. Wang, M. Wang, Buckling of spherical shells subjected to external pressure: a comparison of experimental and theoretical data, Thin-Walled Struct. 111 (2017) 58–64, http://dx.doi.org/10.1016/j.tws.2016.11.012.
[9] O. Ifayefunmi, Buckling behavior of axially compressed cylindrical shells: comparison of theoretical and experimental data, Thin-Walled Struct. 98 (2016) 558–564, http://dx.doi.org/10.1016/j.tws.2015.10.027.
[10] J. Blachut, Buckling of cylinders with imperfect length, J. Press. Vessel Technol. 137 (2014) 011203, http://dx.doi.org/10.1115/1.4027246.
[11] O. Ifayefunmi, J. Błachut, Instabilities in imperfect thick cones subjected to axial compression and external pressure, Mar. Struct. 33 (2013) 297–307, http://dx.doi.org/10.1016/j.marstruc.2013.06.004.
[12] J. Błachut, Combined stability of geometrically imperfect conical shells, Thin-Walled Struct. 67 (2013) 121–128, http://dx.doi.org/10.1016/j.tws.2013.02.007.
[13] J.R. MacKay, F. Van Keulen, M.J. Smith, Quantifying the accuracy of numerical collapse predictions for the design of submarine pressure hulls, Thin-Walled Struct. 49 (2011) 145–156, http://dx.doi.org/10.1016/j.tws.2010.08.015.
[14] S.N. Krivoshapko, Research on general and axisymmetric ellipsoidal shells used as domes, pressure vessels, and tanks, Appl. Mech. Rev. 60 (2007) 336, http://dx.doi.org/10.1115/1.2806278.
[15] P. Jasion, K. Magnucki, Elastic buckling of barrelled shell under external pressure, Thin-Walled Struct. 45 (2007) 393–399, http://dx.doi.org/10.1016/j.tws.2007.04.001.
[16] J. Błachut, Buckling of externally pressurised barrelled shells: a comparison of experiment and theory, Int. J. Press. Vessel. Pip. 79 (2002) 507–517, http://dx.doi.org/10.1016/S0308-0161(02)00040-6.
[17] J. Zhang, M. Wang, W. Wang, W. Tang, Y. Zhu, Investigation on egg-shaped pressure hulls, Mar. Struct. 52 (2017) 50–66, http://dx.doi.org/10.1016/j.marstruc.2016.11.005.
[18] J. Zhang, M. Wang, W. Wang, W. Tang, Buckling of egg-shaped shells subjected to external pressure, Thin-Walled Struct. 113 (2017) 122–128, http://dx.doi.org/10.1016/j.tws.2017.01.017.
[19] J. Blachut, Experimental perspective on the buckling of pressure vessel components, Appl. Mech. Rev. 66 (2013) 011003, http://dx.doi.org/10.1115/1.4026067.
[20] J. Paulose, D.R. Nelson, Buckling pathways in spherical shells with soft spots, Soft Matter 9 (2013) 8227, http://dx.doi.org/10.1039/c3sm50719j.
[21] A. Lee, F. López Jiménez, J. Marthelot, J.W. Hutchinson, P.M. Reis, The geometric role of precisely engineered imperfections on the critical buckling load of spherical elastic shells, J. Appl. Mech. 83 (2016) 1–11, http://dx.doi.org/10.1115/1.4034431.
[22] J. Blachut, P. Wang, Buckling of barreled shells subjected to external hydrostatic pressure, J. Press. Vessel Technol. 123 (2001) 232, http://dx.doi.org/10.1115/1.1357160.
[23] J. Błachut, Optimal barreling of steel shells via simulated annealing algorithm, Comput. Struct. (2003) 1941–1956, http://dx.doi.org/10.1016/S0045-7949(03)00214-1.
[24] P. Jasion, K. Magnucki, Elastic buckling of clothoidal-spherical shells under external pressure - Theoretical study, Thin-Walled Struct. 86 (2015) 18–23, http://dx.doi.org/10.1016/j.tws.2014.10.001.
[25] P. Jasion, Stability analysis of shells of revolution under pressure conditions, Thin-Walled Struct. 47 (2009) 311–317, http://dx.doi.org/10.1016/j.tws.2008.07.005.
[26] K.K. AGRAWAL, B.L. CLARY, E.W. SCHROEDER, Mathematical models of peanut pod geometry, Trans. ASAE (1972) 30.
[27] ENV 1993-1-6: Eurocode 3 – Design of Steel Structures – Part 1.6: Strength and Stability of Shell Structures. Eurocode 3 Part 1.6, CEN, Brussels, 2007.
[28] Rules for the Classification and Construction of Diving Systems and Submersibles. Published by China Classification Society (CCS) in 2013, 2013.
[29] H. Schmidt, Stability of steel shell structures, J. Constr. Steel Res. 55 (2000) 159–181, http://dx.doi.org/10.1016/S0143-974X(99)00084-X.
[30] Z.P. Bazant, L. Cedolin Stability of structures. Mineola, NY: vD.
[31] C. Quillieta, Numerical deflation of beach balls with various Poisson's ratios: from sphere to bowl's shape, Eur. Phys. J. E. 35 (2012), http://dx.doi.org/10.1140/epje/i2012-12048-3.
[32] G.A. Vliegenthart, G. Gompper, Compression, crumpling and collapse of spherical shells and capsules, New J. Phys. 13 (2011), http://dx.doi.org/10.1088/1367-2630/13/4/045020.
[33] J. Błachut, Buckling of externally pressurized steel toriconical shells, Int. J. Press. Vessel. Pip. 144 (2016) 25–34, http://dx.doi.org/10.1016/j.ijpvp.2016.05.002.
[34] D. Vella, A. Ajdari, A. Vaziri, A. Boudaoud, The indentation of pressurized elastic shells: from polymeric capsules to yeast cells, J. R. Soc. Interface 9 (2012) 448–455, http://dx.doi.org/10.1098/rsif.2011.0352.
[35] D.A. Fletcher, R.D. Mullins, Cell mechanics and the cytoskeleton, Nature 463 (2010) 485–492, http://dx.doi.org/10.1038/nature08908.
[36] E. Katifori, S. Alben, E. Cerda, D.R. Nelson, J. Dumais, Foldable structures and the natural design of pollen grains, Proc. Natl. Acad. Sci. USA 107 (2010) 7635–7639, http://dx.doi.org/10.1073/pnas.0911223107.
[37] A. Lazarus, H.C.B. Florijn, P.M. Reis, Geometry-induced rigidity in nonspherical pressurized elastic shells, Phys. Rev. Lett. 109 (2012), http://dx.doi.org/10.1103/PhysRevLett.109.144301.
[38] T.S. Baker, N.H. Olson, S.D. Fuller, Adding the third dimension to virus life cycles: three-dimensional reconstruction of icosahedral viruses from cryo-electron micrographs, Microbiol. Mol. Biol. Rev. 63 (1999) 862–922, http://dx.doi.org/10.1128/MMBR.64.1.237-237.2000 (table of contents).